

Fast Mølmer-Sørensen gates in trapped-ion quantum processors with compensated carrier transition

Evgeny Anikin,¹ Andrey Chuchalin,^{1, 2} Nikita Morozov,¹ Olga Lakhmanskaya,¹ and Kirill Lakhmanskij¹

¹*Russian Quantum Center, Skolkovo, Moscow 143025, Russia*

²*Moscow Institute of Physics and Technology, Dolgoprudny, 141700, Russia*

(Dated: January 7, 2025)

Carrier transition is one of the major factors hindering the high-speed implementation of Mølmer-Sørensen gates in trapped-ion quantum processors. We present an approach to design laser pulse shapes for Mølmer-Sørensen gate in ion chains which accounts for the effect of carrier transition on qubit-phonon dynamics. We show that the fast-oscillating carrier term effectively modifies the spin-dependent forces acting on ions, and this can be compensated by a simple nonlinear transformation of a laser pulse. Using numerical simulations for short ion chains and perturbation theory for longer chains, we demonstrate that our approach allows to reach the infidelity below 10^{-4} while keeping the gate duration below $100\mu\text{s}$.

I. INTRODUCTION

High-fidelity entangling gates are critical for the practical realization of quantum computers. With cold trapped ions, remarkable progress in gate implementation has been achieved in recent decades [1]. Since Cirac-Zoller gate [2], various gate designs have been proposed and implemented, including Mølmer-Sørensen gate [3], light-shift gate [4], ultrafast gates [5], etc. Among them, Mølmer-Sørensen gate and its variations are the most ubiquitous.

Mølmer-Sørensen gate (MS gate) is implemented with the help of a bichromatic external field pulse, typically an optical or Raman laser beam, detuned symmetrically from the qubit transition [3]. In Lamb-Dicke regime, the field creates a spin-dependent force acting on ions, and the pulse parameters should be chosen to make ion trajectories closed curves in phase space. As a result, qubits acquire a spin-dependent phase and become entangled.

For a two-ion crystal, high-fidelity MS gates can be implemented with constant-amplitude field smoothly turned on and off [6]. For larger ion number, more complicated pulse shapes are required in order to close phase space trajectories for multiple motional modes of an ion crystal [7]. For amplitude-modulated pulses, the pulse shape is determined by a set of linear equations [7] which can be efficiently solved numerically.

In recent literature, a variety of pulse shaping approaches have been proposed for different purposes. Apart from amplitude modulation proposed in [7], phase modulation [8] and multi-tone beams [9] can be used. Also, additional constraints on the pulse shape allow to implement parallel gates [10, 13], to enhance gate robustness against fluctuations of the experimental parameters [11, 12], or to minimize the total external field power [11].

To design laser pulses implementing MS gate with highest possible fidelity, a careful error analysis is necessary. The errors originate both from technical noises, such as laser and magnetic field fluctuations, and the intrinsic laser-ion interactions [14]. To account for the

latter, it is necessary to go beyond the usual simplifying assumptions such as Lamb-Dicke and rotating-wave approximations often used to describe laser-ion dynamics. The latter can be achieved by a numerical simulation in the full ion-phonon Hilbert space or by applying a systematical procedure such as Magnus expansion beyond the leading order [15, 16].

One of the unwanted interactions present in trapped ions is the carrier transition. It is present when a bichromatic beam with two co-propagating plane wave components acts on ion qubits. Although for the MS gate operation the beam components should be close to qubit motional sidebands, direct qubit transition is also inevitably present. Its influence grows with increasing gate speed [6], and it becomes one of the dominant factors limiting gate fidelity at short gate times [14].

The theoretical analysis of ion dynamics with full account for carrier term has been performed for two ions interacting with a single phonon mode [6, 17]. It has been shown that the fast-oscillating carrier term results in a nonlinear renormalization of the driving field amplitude, and (for strictly rectangular pulse) in a basis rotation of the $R_{XX}(\theta)$ gate operator depending on the relative phase between the bichromatic beam components. For gate implementation in long chains, multiple phonon modes should be considered, and amplitude pulse shaping should ensure closed phase-space motional trajectories.

In this work, we present a theoretical analysis of the influence of carrier transition on MS gate dynamics in a multi-ion chain with account for all phonon modes. For amplitude-shaped pulse, we eliminate the carrier term in the system Hamiltonian by going into interaction picture. The leading part of the resulting Hamiltonian has the form of a spin-dependent force Hamiltonian, where carrier transition modifies the force values obtained from Lamb-Dicke expansion. We propose a family of pulse shapes which takes into account this modification. Our pulses can be found by applying a simple nonlinear transformation to a pulse obtained from linear equations. Using numerical simulations for short chains and perturba-

tion theory calculations for longer chains, we demonstrate that our pulse-shaping scheme shows a considerable fidelity gain in comparison to pulses obtained from linear equations for gate times 50-100 microseconds and 2-20 ions, and the theoretical infidelity for our pulses is below 10^{-4} .

So, our pulse-shaping approach provides a considerable speedup while maintaining high gate fidelity, which is a step towards meeting the challenging requirements for practical quantum computations.

II. DYNAMICS OF TRAPPED IONS QUBITS IN THE PRESENCE OF CARRIER TRANSITION

We consider the trapped-ion quantum processor consisting of a system of ions confined in a radio frequency Paul trap, where two electronic levels of each ion constitute qubit levels. We assume that ions form a linear crystal, therefore, ions share independent sets of collective phonon modes for each trap axis directions [18]. We consider the implementation of an entangling gate between two ion qubits with an amplitude-modulated bichromatic laser field symmetrically detuned from qubit transition. The interaction-picture Hamiltonian for the considered pair of ions reads [19]

$$\hat{H} = -i \sum_{i=1,2} \Omega(t) \cos(\mu t + \psi) (e^{ik_a \hat{r}_{ia}} \sigma_+^i - \text{h.c.}), \quad (1)$$

where k_a are the components of the laser field wavevector, \hat{r}_{ia} are the components of ions displacements from their equilibrium positions, $k_a \hat{r}_{ia} = \sum_m \eta_{im} (\hat{a}_m e^{-i\omega_m t} + \hat{a}_m^\dagger e^{i\omega_m t})$, \hat{a}_m and \hat{a}_m^\dagger are the creation and annihilation operators of the phonon modes, ω_m are the phonon mode frequencies, η_{im} are the Lamb-Dicke parameters, and $\Omega(t)$ is the bichromatic beam amplitude envelope. For the implementation of the target entangling gate, which we specify as the $R_{XX}(\phi) = \exp\{-i\phi \sigma_x \otimes \sigma_x\}$ gate, one should find a pulse $\Omega(t)$ that the system evolution operator reduces to the target gate operator.

To find the approximate evolution operator, one can expand the system Hamiltonian in the Lamb-Dicke parameters. Up to the first order, the Hamiltonian reads

$$\hat{H} = \hat{H}_0 + \hat{H}_1, \quad (2)$$

where

$$\hat{H}_0 = \sum_i \Omega(t) \cos(\mu t + \psi) \sigma_y^i. \quad (3)$$

$$\hat{H}_1 = \sum_{i,m} \eta_{im} \Omega(t) \cos(\mu t + \psi) (a_m e^{-i\omega_m t} + a_m^\dagger e^{i\omega_m t}) \sigma_x^i \quad (4)$$

The Hamiltonian in Lamb-Dicke approximation contains two contributions H_0 and H_1 . The term H_1 is a

spin-dependent force Hamiltonian [20, 21]. The term H_0 corresponds to direct carrier transitions. Often, the contribution of \hat{H}_0 is neglected. This approximation is valid when μ is close to one or several phonon mode frequencies, so \hat{H}_1 contains slowly-oscillating terms which contribute the dynamics significantly, whereas \hat{H}_0 is fastly oscillating.

The evolution operator for the spin-dependent force Hamiltonian \hat{H}_1 reads [21]

$$U_{\text{MS}}(t_1, t_2) = \exp \left(-\frac{i}{2} \sum_{i,j} \chi_{ij}^0(t_2, t_1) \sigma_x^i \sigma_x^j \right) \prod_m D_m \left(\sum_i \sigma_x^i \alpha_{i,m}^0(t_2, t_1) \right), \quad (5)$$

where

$$\alpha_{im}^0(t_2, t_1) = -i \int_{t_1}^{t_2} f_{im}^0(t') dt' \quad (6)$$

$$\chi_{ij}^0(t_2, t_1) = \text{Re} \int_{t_1}^{t_2} [\alpha_{im}^0(t', t_1) (f_{jm}^0)^*(t') + (\alpha_{jm}^0)^* f_{im}^0] dt' \quad (7)$$

$$f_{im}^0(t) = \eta_{im} e^{i\omega_m t} \Omega(t) \cos(\mu t + \psi). \quad (8)$$

For the implementation of an $R_{XX}(\theta)$ gate, an appropriate pulse shape $\Omega(t)$ should be found. Let $\Omega(t)$ be applied in the time interval (t_0, t_f) . By comparing the target $R_{XX}(\theta)$ operator with the evolution operator (5), one gets the following conditions for α_{im}^0 and χ_{ij}^0 [7, 21]:

$$\alpha_{im}^0(t_f, t_0) = 0, \quad (9)$$

$$\chi_{12}^0(t_f, t_0) = \phi. \quad (10)$$

The equations (9) comprise $2n_{ions}$ linear equations for $\Omega(t)$. The equations (9) can be solved by numerically by standard linear algebra routines. With approximations made, the resulting $\Omega(t)$ implements the MS gate with 100% fidelity.

However, even in the absence of technical noises, the neglected term \hat{H}_0 contributes to gate infidelity, and its importance grows with increasing gate speed. To account for the carrier term systematically, let us go into interaction picture with respect to H_0 :

$$|\psi\rangle = e^{-i \int_{t_0}^t \hat{H}_0(t') dt'} |\psi_{Ic}\rangle = e^{-i\Phi(t) \sum_i \sigma_y^i} |\psi_{Ic}\rangle, \quad (11)$$

where

$$\Phi(t) = \int_{t_0}^t dt' \Omega(t') \cos(\mu t' + \psi). \quad (12)$$

After this transformation the Hamiltonian takes form

$$\hat{H}_{Ic} = \sum_{i,m} \eta_{im} \Omega(t) \cos(\mu t + \psi) (a_m e^{-i\omega_m t} + a_m^\dagger e^{i\omega_m t}) \times \underbrace{\cos 2\Phi(t) \sigma_x^i}_{\text{leading-order}} + \underbrace{\sin 2\Phi(t) \sigma_z^i}. \quad (13)$$

The transformation (11) is equivalent to the single-qubit rotations applied after the gate operation. These rotations could be compensated by applying additional resonant pulses after the gate operation. However, this is not necessary because the rotation angle $\Phi(t_f)$ can be greatly reduced by appropriate pulse design. In the following, we assume that $\Omega(t)$ satisfies the following conditions:

1. $\Omega(t)$ varies slowly in comparison to μ^{-1} ,
2. $\Omega(t)$ and its first derivatives vanish in the beginning and in the end of the pulse.

Under these conditions and with our proposed pulse design (described in more detail in subsequent sections), we get typical values of $\Phi(t_f)$ of order 10^{-5} - 10^{-4} . Therefore, we can assume that the final state of the qubit-phonon system is determined only by evolution with the Hamiltonian (13).

To analyze the Hamiltonian (13), we suggest to split it into two parts, the leading order part $\hat{H}_{Ic}^{(0)}$ and the perturbation part \hat{V} , as shown by underbraces. The perturbation alone reads

$$\hat{V} = \sum_{i,m} \eta_{im} \Omega(t) \cos(\mu t + \psi) \sin 2\Phi(t) \times (a_m e^{-i\omega_m t} + a_m^\dagger e^{i\omega_m t}) \sigma_z^i. \quad (14)$$

Such a decomposition is justified under two assumptions on $\Phi(t)$:

1. $\Phi(t)$ oscillates near zero;
2. its magnitude remains $\lesssim 1$.

These assumptions hold for all the pulses that will be considered below. With these assumptions, the $\cos 2\Phi(t)$ term oscillates near ~ 1 and gives a contribution important on large time scales. In contrast, $\sin 2\Phi(t)$ oscillates near zero, so its contribution cancels on large time scales. Because of that, it is reasonable to consider the sine term as a perturbation.

The leading-order term \hat{H}_0 has the form of a spin-dependent forces Hamiltonian, so its propagator has the same form as (5):

$$U_0(t_1, t_2) = \exp \left(-\frac{i}{2} \sum_{i,j} \chi_{i,j}(t_2, t_1) \sigma_x^i \sigma_x^j \right) \prod_m D_m \left(\sum_i \sigma_x^i \alpha_{i,m}(t_2, t_1) \right), \quad (15)$$

where

$$\alpha_{im}(t_2, t_1) = -i \int_{t_1}^{t_2} f_{im}(t') dt' \quad (16)$$

$$\chi_{ij}(t_2, t_1) = \text{Re} \int_{t_1}^{t_2} [\alpha_{im} f_{jm}^* + \alpha_{jm}^* f_{im}] dt' \quad (17)$$

$$f_{im}(t) = f_{im}^0(t) \underbrace{\cos 2\Phi(t)}_{\text{carrier effect}}, \quad (18)$$

Because of the transformation into the interaction picture generated by the carrier term, the spin-dependent forces $f_{im}(t)$ get an additional $\cos 2\Phi(t)$ term.

In addition, the evolution operator is modified by perturbative corrections generated by \hat{V} . Within the first-order perturbation theory by \hat{V} , the evolution operator of the Hamiltonian (13) can be expressed as

$$\hat{U} = \hat{U}_0 \left(\mathbb{1} - i \hat{T}_1 \right), \quad (19)$$

where

$$\hat{T}_1 = \int_{t_0}^{t_f} \hat{U}_0^\dagger(t', t_0) \hat{V} \hat{U}_0(t', t_0) dt'. \quad (20)$$

As the perturbation \hat{V} contains the sigma matrices σ_z^i , the operator \hat{T}_1 causes the spin flip processes in x -basis: for the initial qubit state $|s_1 s_2\rangle_x$ (Pauli string in x -basis), it causes transitions to another Pauli string $|s'_1 s'_2\rangle_x$ which differs from the initial state by a single spin flip. However, in the next sections, we show that these processes cause only a small correction to the system evolution for the considered pulses. Therefore, we can use the expression (15) for the description of gate dynamics and for the determination of the pulse shape $\Omega(t)$.

With modified expressions for spin-dependent forces, we get new conditions for the implementation of $R_{XX}(\phi)$:

$$\begin{aligned} \alpha_{im}(t_f, t_0) &= 0, \\ \chi_{12}(t_f, t_0) &= \phi. \end{aligned} \quad (21)$$

The definitions of α_{im} and χ_{ij} differ from α_{im}^0 and χ_{ij}^0 by the $\cos 2\Phi(t)$ term, where $\Phi(t)$ is expressed as an integral (12) containing $\Omega(t)$. Because of that, the Eqs. (21) become nonlinear integral equations in contrast to the linear equations (9). In Section (IV), we present an approximate scheme for solving these equations.

III. CONTRIBUTIONS OF CARRIER TERM TO GATE INFIDELITY

The expressions (15) and (19) for the propagator can be used for analytical calculation of the gate fidelity of an ion chain of arbitrary length. In this section, we present

the expressions for the gate fidelity defined in the full ion-phonon Hilbert space. We assume that the ion chain is cooled to the ground state at the beginning of the gate operation, so the initial state of the qubit-phonon system is $|\psi_0\rangle \equiv |\psi_{0q}\rangle \otimes |0_{\text{ph}}\rangle$, where $|\psi_{0q}\rangle$ is the initial qubit state. The action of the ideal $R_{\text{XX}}(\phi)$ gate turns qubits into the state $R_{\text{XX}}(\phi)|\psi_{0q}\rangle$ but leaves all phonon modes in the ground state. Therefore, we can characterize the gate realization by fidelity between the state $|\psi_t\rangle \equiv R_{\text{XX}}(\phi)|\psi_0\rangle$ (the outcome of the ideal $R_{\text{XX}}(\phi)$ gate) and the state $|\psi(t_f)\rangle = \hat{U}|\psi_0\rangle$ obtained after the evolution with the Hamiltonian (1):

$$F = |\langle\psi_t|\psi(t_f)\rangle|^2 = |\langle\psi_0|R_{\text{XX}}(\phi)^\dagger U|\psi_0\rangle|^2. \quad (22)$$

Due to imperfect pulse design, $\alpha_{im}(t_f, t_0)$ and $\chi_{12}(t_f, t_0)$ may deviate from target values of Eq. (21) in the end of the gate. Because of that, already the leading-order term of the evolution operator \hat{U}_0 will not coincide with the ideal $R_{\text{XX}}(\phi)$ operator. So, it is meaningful to define another fidelity measure F_0 (zero-order fidelity) obtained from the leading-order propagator \hat{U}_0 :

$$F_0 \equiv |\langle\psi_0|R_{\text{XX}}^\dagger(\phi)U_0|\psi_0\rangle|^2 \quad (23)$$

In Appendix B, we find F_0 for various initial states $|\psi_{0q}\rangle$. In particular, for $|\psi_{0q}\rangle = |s_1s_2\rangle_z$ (Pauli strings in the z -basis, $s_i = \pm 1$), the infidelity reads

$$1 - F_0 \approx \sum_{im} |\alpha_{im}(t_f)|^2 + \Delta\chi_{12}(t_f)^2, \quad (24)$$

where $\Delta\chi_{12}(t_f) = \phi - \chi_{12}(t_f)$. We see that incomplete closure of the phase trajectories and the error in the angle ϕ give two additive contributions into the average gate infidelity. Our expressions slightly differ from [14], [21] due to our different fidelity definition.

Also, for $|\psi_{0q}\rangle = |s_1s_2\rangle_x$ (Pauli strings in z -basis), zero-order gate infidelity is given by expression

$$1 - F_0 = P_{\text{ph}}(s) = \sum_m \left| \sum_i \alpha_{im} s_i \right|^2. \quad (25)$$

In this case, the error in ϕ does not contribute to gate fidelity. At small α_{im} , the infidelity can be interpreted as the probability of phonon excitation after the gate operation.

Then, let us find the contribution to infidelity caused by the spin-flip perturbation accounted by the \hat{T}_1 term in the evolution operator (19). For simplicity, we consider only the initial states $|\psi_0\rangle = |s_1s_2\rangle_x$. The spin flip probability for such initial states is

$$P_{\text{flip}}^s = \langle s, 0_{\text{ph}} | T_1^\dagger T_1 | s, 0_{\text{ph}} \rangle. \quad (26)$$

In Appendices B and C, we derive the explicit expression (C8) for P_s as a two-dimensional integral over time. The integral (C8) is suitable for the calculation of the spin flip

probability for long ion chains where the full numerical solution is not feasible.

Also, we show that the gate infidelity for the initial states $|s_1s_2\rangle_x$ with account for the carrier transition reads

$$1 - F = P_{\text{ph}}^s + P_{\text{flip}}^s, \quad (27)$$

so the contributions of imperfectly closed phase trajectories and spin flip error are additive. For other qubit states, there are interference terms between the two considered contributions into error.

Finally, we show that the infidelity averaged over all initial qubit states over the Fubini-Study measure:

$$1 - \langle F \rangle < 1 - \langle F_0 \rangle + \frac{1}{4} \sum_s P_s, \quad (28)$$

where F_0 given by Eq. (23) accounts only for the leading-order term of \hat{U} . Therefore, it is sufficient to calculate the contribution of \hat{T}_1 only for the initial states $|s_1s_2\rangle_x$ to find an upper bound for the average gate infidelity.

Thus, carrier term contributes into two types of gate error. First, it modifies the values of the spin-dependent forces, so it causes incomplete closing of the phase trajectories unless the pulse shape is chosen appropriately. Second, it causes the spin-flip error arising from \hat{T}_1 . In the following, we present a method to find pulses which approximately close the phase trajectories with account for the modification of the spin-dependent forces by carrier term.

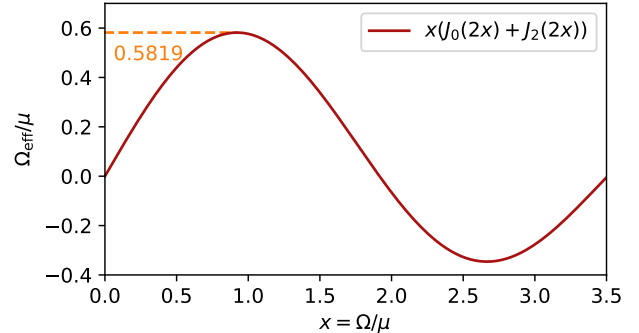


Figure 1. (a) The dependence of the effective Rabi frequency $\Omega_{\text{eff}}(t)$ on Ω given by Eq. (30).

IV. PULSE SHAPING SCHEME

In this section, we present a method to find pulse shapes which approximately satisfy the Eqs. (21). Then, we demonstrate its performance on a particular example of a 5-ion chain and compare the pulse obtained by our method with the pulse obtained from linear Eqs. (9), (10). We show that it strongly reduces the contribution of α_{im} and $\Delta\chi_{12}$ to the zero-order infidelity $1 - F_0$, thus increasing the overall fidelity.

	$\Omega_{\text{tr}}(t)$	$\Omega_{\text{lin}}(t)$
$1 - F_0$	1.426×10^{-6}	1.237×10^{-2}
Num. (LD)	1.652×10^{-6}	1.246×10^{-2}
Num. (full)	5.687×10^{-5}	1.384×10^{-2}

Table I. $R_{\text{XX}}(\pi/4)$ gate fidelity for the pulses Ω_{lin} and Ω_{tr} with the initial state $|11\rangle_z$. The values in the first row are obtained from the analytical expression (24). The values in the second and third row are obtained from TDSE solution with the Hamiltonians (2) and (1).

Assume that $\Omega(t)$ satisfies the smoothness conditions from Section II, so it varies slowly on the timescale μ^{-1} and is smoothly turned on (off) at the beginning (end) of the gate. Then, the $\cos 2\Phi(t)$ term in Eq. (18) can be approximately averaged over fast oscillations on the timescale μ^{-1} . In Appendix D, we demonstrate that averaging allows to replace f_{im} in Eq. (18) with

$$f_{im} \approx \eta_{im} e^{i\omega_m t} \Omega_{\text{eff}}(t) \cos(\mu t + \psi), \quad (29)$$

where

$$\Omega_{\text{eff}}(t) = \mathcal{S}(\Omega(t)) = \Omega(t) \left(J_0 \left(\frac{2\Omega(t)}{\mu} \right) + J_2 \left(\frac{2\Omega(t)}{\mu} \right) \right), \quad (30)$$

and J_k are Bessel functions. As a result, the $\cos 2\Phi(t)$ term in Eqs.(16), (17) causing the nonlinearity of Eqs. (21) disappears. Thus, α_{im} and χ_{ij} can be calculated with Eqs. (6), (7) as there were no carrier term, but with $\Omega(t)$ replaced by $\Omega_{\text{eff}}(t)$.

The transformation $\mathcal{S}(\Omega)$ given by Eq. (30) can be thought as a nonlinear squeezing transformation of $\Omega(t)$. In Fig. 1), we depict the functional dependence of $\mathcal{S}(\Omega)$ on Ω . When $\Omega \ll \mu$, $\mathcal{S}(\Omega) \approx \Omega$. At larger $\Omega \sim \mu$, $\mathcal{S}(\Omega)$ grows slower than Ω until it reaches its absolute maximum $\max(\mathcal{S}) = C\mu$, where $C \approx 0.581865$. At even larger Ω , $\mathcal{S}(\Omega)$ has an oscillatory dependence on Ω . This behavior of $\mathcal{S}(\Omega)$ shows that the presence of the carrier term effectively reduces the field amplitude acting on an ion qubit.

With knowledge of the transformation (30), we can find approximate solutions of the nonlinear equations (21) in two simple steps:

1. With account for the smoothness conditions, find a solution $\Omega_{\text{lin}}(t)$ of Eqs. (9), (10), where α_{im}^0 and χ_{ij}^0 are defined by Eqs. (6), (7), (8).
2. The obtained solution should be taken as Ω_{eff} in Eq. (30): so, the approximate solution of Eqs. (21) is $\Omega_{\text{tr}}(t) = \mathcal{S}^{-1}(\Omega_{\text{lin}}(t))$.

The pulse $\Omega_{\text{lin}}(t)$ obtained after the step 1 would implement the $R_{\text{XX}}(\phi)$ gate if the carrier term was not present. By the step 2, $\Omega_{\text{lin}}(t)$ is transformed to account for the modified expressions for the spin-dependent forces.

Let us illustrate the presented pulse shaping scheme on a particular example. We consider a chain of $n_{\text{ions}} = 5$

$^{40}\text{Ca}^+$ ions in a harmonic pseudopotential with radial frequency of 1 MHz and the axial frequency of 264.8 kHz. The frequency of the lowest radial mode at these parameters is 0.75 MHz. We calculate the ion equilibrium positions, phonon normal modes and frequencies and Lamb-Dicke parameters of the chain using standard methods [18] (see Fig.2a-c). Then, we find the pulses implementing the $R_{\text{XX}}(\phi = \pi/4)$ gate between the second and the third ions of the chain for the gate time 41.74 μs , the detuning $\mu = 2\pi \times 1.034$ MHz, and the motional phase $\psi = 0$.

First, we find a solution $\Omega_{\text{lin}}(t)$ of Eqs. (9), (10), satisfying the smoothness conditions of the Section II. We split the interval (t_0, t_f) into $2n_{\text{ions}} + 2 = 12$ equal segments and search for Ω_{lin} as a piecewise-cubic polynomial (cubic spline). We require continuity up to the first-order derivatives and vanishing values and derivatives at the beginning and at the end of the gate. Under these requirements, Eqs. (9), (10) have a unique solution (see Appendix A). Then, we apply the inverse transformation (30) to find $\Omega_{\text{tr}}(t)$. For the considered 5-ion chain, $\Omega_{\text{lin}}(t)$ and $\Omega_{\text{tr}}(t)$ are shown in Fig. 2c.

For both pulses ($\Omega_{\text{lin}}(t)$ and $\Omega_{\text{tr}}(t)$) we consider the system dynamics during the gate. Using Eqs. (16), (17), we find $\alpha_{im}(t, t_i)$ and $\chi_{ij}(t, t_i)$ entering the propagator (15). For the center-of-mass (COM) and stretch modes of an ion crystal, the phase trajectories are shown in Fig. 2e, and the time dependence of χ_{12} is shown in Fig. 2f. From Fig. 2e, it is clear that the phonon mode trajectories are not perfectly closed for the pulse $\Omega_{\text{lin}}(t)$. In contrast, for $\Omega_{\text{tr}}(t)$ they are almost perfectly closed. Also, the value of χ_{12} at the end of the gate for $\Omega_{\text{lin}}(t)$ significantly deviates from the target value of $\pi/4$, whereas the deviation is much smaller for $\Omega_{\text{tr}}(t)$.

The calculated values of α_{im} and $\Delta\chi_{12}$ at the end of the gate allow to predict the gate infidelity without the spin-flip contribution using Eq. (24). For the initial $|11\rangle_z$ state, the results are presented in Table I. One can see that the theoretical infidelity for the pulse Ω_{tr} is $\sim 10^{-6}$, which is in agreement with almost perfect phase trajectory closing shown in Fig. 2e and the correct value of $\chi_{12}(t_f, t_0)$. In contrast, the predicted infidelity for the pulse Ω_{lin} is of order $\sim 10^{-2}$.

To verify these predictions, we solve numerically the time-dependent Schrödinger equation (TDSE) for the Hamiltonian (1) using QuTiP [22]. The calculated infidelities for both pulses are also in Table I. For Ω_{lin} , the infidelity is slightly higher than the theoretical prediction, but also of order 10^{-2} . For Ω_{tr} , the infidelity is approximately $6 \cdot 10^{-5}$, which is more than two orders of magnitude lower than for Ω_{lin} . However, it is more than order of magnitude higher than the analytical value. We attribute this difference to the higher-order terms in the Lamb-Dicke parameters, which are not taken into account by our calculations but are present in the full Hamiltonian (1). To confirm this, we also solve TDSE for the Hamiltonian (2), where the higher-order terms of the expansion are neglected. The results, also presented

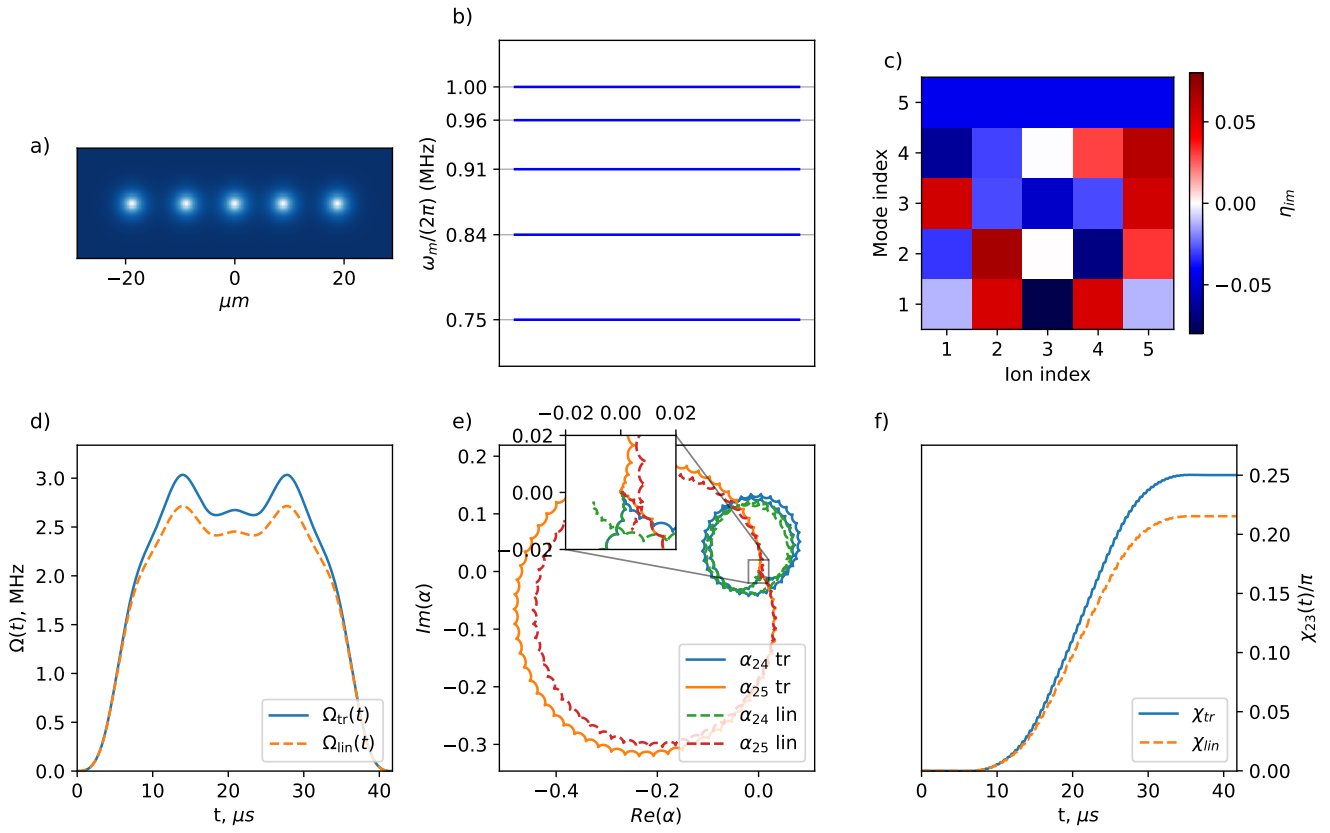


Figure 2. (a-c) Ion equilibrium positions, radial frequencies and normal modes of a 5-ion $^{40}\text{Ca}^+$ chain (d) Non-optimized and optimized laser pulses applied to ions 2 and 3 (e) Phase trajectories for modes 4 (stretch) and 5 (COM) for both pulses (f) $\chi_{23}(t)$ for both pulses

		Ω_{tr}			Ω_{lin}		
		Eq. (27)	Num. (LD)	Num. (full)	Eq. (27)	Num. (LD)	Num. (full)
$ 1, 1\rangle_x$	P_{ph}^s	1.916×10^{-6}	8.547×10^{-7}	3.405×10^{-6}	8.766×10^{-4}	8.958×10^{-4}	9.673×10^{-4}
	P_{flip}^s	9.265×10^{-7}	8.741×10^{-7}	6.593×10^{-6}	3.578×10^{-7}	3.296×10^{-7}	3.600×10^{-6}
	$1 - F$	2.843×10^{-6}	1.777×10^{-6}	1.008×10^{-5}	8.770×10^{-4}	8.962×10^{-4}	9.710×10^{-4}
$ 1, -1\rangle_x$	P_{ph}^s	6.347×10^{-7}	4.649×10^{-7}	1.072×10^{-6}	1.080×10^{-4}	1.094×10^{-4}	1.036×10^{-4}
	P_{flip}^s	5.685×10^{-7}	5.253×10^{-7}	3.459×10^{-6}	2.464×10^{-7}	2.202×10^{-7}	2.182×10^{-6}
	$1 - F$	1.203×10^{-6}	1.186×10^{-6}	4.704×10^{-6}	1.083×10^{-4}	1.097×10^{-4}	1.058×10^{-4}

Table II. Contributions into $R_{XX}(\pi/4)$ gate fidelity for the pulses Ω_{lin} and Ω_{tr} with the initial states $|1, \pm 1\rangle_x$. Each data row of the table corresponds to a contribution to the infidelity with the initial state given in the leftmost column. Each data column of the table corresponds to a calculation method (analytical or numerical with one of the considered Hamiltonians) for the pulse given in the top row.

in Table I, show better agreement with the analytical predictions. The discrepancy in this case can be attributed to the higher orders of the perturbation theory in \hat{V} .

In addition, we analyze the gate fidelity for the initial states $|s_1 s_2\rangle_x$. In this case, Eq. (27) allows to separate the contributions of imperfectly closed phase trajectories and spin flips. Also, these contributions can be identified from numerical solution of TDSE: the first term in Eq. (27) equals the probability of phonon mode excitation, and the second term equals the probability of a spin

flip. Both these probabilities can be extracted from the TDSE solution. In Table II, we present the results of analytical calculations and TDSE solution with both types of Hamiltonians for the initial states $|1, \pm 1\rangle_x$.

The results confirm that the first-order perturbation theory in \hat{V} gives an accurate description of the dynamics with the first-order Hamiltonian (2). Indeed, for Ω_{lin} , the probabilities P_{ph}^s and P_{flip}^s calculated analytically and numerically are in good agreement. For Ω_{tr} , the spin flip probability P_{flip}^s is also accurately predicted by the an-

alytical formula. The analytical formula for P_{ph}^s is less accurate, but it predicts correctly the very small magnitude of phonon excitation probability, 10^{-6} .

For the simulation of the full Hamiltonian (1) with pulses Ω_{lin} , the considered contribution into error again match with the analytical predictions. However, for Ω_{tr} , both of the contributions are by order of magnitude larger than the corresponding analytical predictions. Still, the total error for Ω_{tr} is more than by order of magnitude lower than for Ω_{lin} .

From these results, we conclude that the dominant contributions into gate error for Ω_{lin} are indeed given by Eq. (24). These contributions, namely the error $\Delta\chi_{12}$ in the rotation angle and the imperfect closing of the phase trajectories, can be almost canceled by transforming Ω_{lin} into Ω_{tr} . The spin-flip contribution gives a negligibly small contribution into error for both pulses. Thus, the pulse Ω_{tr} allows the implementation of a fast high-fidelity $R_{\text{XX}}(\pi/4)$ gate in a 5-ion chain.

V. CALCULATIONS

The results of the previous section can be used to implement a fast high-fidelity $R_{\text{XX}}(\pi/4)$ gate in a five-ion chain for a particular gate time and bichromatic detuning. Now let us examine the applicability of the method for other gate times, detunings, and chain lengths. Below, we find the parameter domains for which the method of Section IV can be implemented. For the 5-ion chain considered previously, we perform analytical and numerical calculations for different parameter values and study the fidelity dependence on these parameters. For longer ion chains which cannot be treated numerically, we perform only analytical calculations.

The transformation \mathcal{S}^{-1} proposed in IV acts on pulses Ω_{lin} obtained with the usual pulse shaping approach with additional smoothness requirements. These pulses depend on the number of ions, the values of normal mode frequencies, the Lamb-Dicke parameters, the detuning of the bichromatic beam, the gate time and the additional requirements for the pulse shape. The normal mode frequencies and the Lamb-Dicke parameters depend on the trap frequencies, ion masses and the wavevectors, however, these dependencies are rather simple and do not contain fastly oscillating contributions. In contrast, the dependence on t_{gate} and μ is highly non-trivial because they enter the pulse shaping equations inside the oscillatory integrals (A2). The dependence on the motional phase ψ is weak providing that the field amplitude is smoothly turned on and off. Therefore, we mostly focus on the dependence on t_{gate} and μ .

A key point for the implementation of our scheme is the existence of the inverse transformation \mathcal{S}^{-1} . As shown in previous section (see Eq. (30) and Fig. 1), the effective field amplitude Ω_{eff} has an absolute maximum of $C\mu$: therefore, \mathcal{S}^{-1} is defined only in the range $(-C\mu, C\mu)$. So, for the step 2 of the pulse shaping procedure in Sec-

tion IV, it is necessary that the absolute value of Ω_{lin} obtained from linear equations does not exceed $C\mu$. It is useful to find the set of parameters t_{gate} and μ for which this condition is satisfied. Below we call such sets on the plane (t_{gate}, μ) allowed areas. As shown below, allowed areas have complicated shape due to the nontrivial dependence of Ω_{lin} on t_{gate} and μ .

First, we find the allowed area for the 5-ion chain considered in the previous section. For that, we calculate $\Omega_{\text{lin}}(t)$ for a sufficiently dense grid in $t_{\text{gate}}-\mu$ plane (1450×800) for gate times from 5 to $150 \mu\text{s}$ and detunings from 0.6 to 1.2MHz. The area is shown by color in Fig. 3a with its border indicated by a solid line. Along the vertical axis, the area occupies the values of μ lying closely to the band of radial phonon frequencies. Along the horizontal axis, it spans the whole range of t_{gate} except the values below $\sim 30\mu\text{s}$.

For each point inside the allowed area, we also calculate the transformed pulse $\Omega_{\text{tr}}(t)$. Using Eq. (24), we calculate the leading-order contribution $1 - F_0$ to gate infidelity for the initial state $|11\rangle_z$ for each pair t_{gate}, μ . The result is shown in Fig. 3a by color. We find that infidelity is of order 10^{-5} nearly for all points inside the area except the vicinity of the boundaries.

For comparison, we calculate $1 - F_0$ for pulses Ω_{lin} with the initial state $|11\rangle_z$ in the entire grid. The result is shown in Fig 3(c). We find that the infidelity for Ω_{lin} is considerably larger than for Ω_{tr} inside the allowed area and it becomes even larger outside it.

We also perform these calculations for a 20-ion chain. All laser and trap parameters are taken the same as for 5-ion case except the axial frequency, which is set to 78.7kHz, and the number of segments in the pulse, which is $2n_{\text{ions}} + 1 = 41$. With such value of axial frequency, radial phonon modes are all in the range (0.75MHz, 1MHz) as for the 5-ion case. In Fig. 3(b,d), we show the results for a 20-ion chain. Analogously with the 5-ion case, we find the allowed area and calculate $1 - F_0$ for Ω_{lin} and Ω_{tr} in the t_{gate}, μ plane. The 20-ion allowed area (see Fig. 3(b)) has a shape similar to the 5-ion case, however, it is shifted to larger gate times: the minimal time for points inside the area is $\sim 60\mu\text{s}$. Analogously with the 5-ion case, we find that $1 - F_0$ is of order 10^{-5} for Ω_{tr} (see Fig. 3(b)) and of order 10^{-2} for Ω_{lin} (see Fig. 3(d)).

For other chain lengths from 2 to 20, we get analogous results. In Fig. 5, we show the dependence of the minimal time (t_{min}) inside the allowed area on the number of ions. Also, for each n_{ions} , we find the minimal gate time for which $1 - F_0$ reaches 10^{-5} (t_{min}^*). Both of these times grow monotonically with the increasing number of ions, with t_{min}^* exceeding t_{min} no more than by $\sim 20\mu\text{s}$.

Also, we calculate analytically the spin flip probability for a selected set of points in t_{gate}, μ plane inside the area for 5-ion and 20-ion chains with the initial state $|11\rangle_x$. The points are shown in Fig. 3(a) (5 ions) and Fig. 3(b) (20 ions). The values of the spin flip probability are shown in Fig. 3(e) and Fig. 3(f). For all selected points, the spin flip probability for a 5-ion chain does not

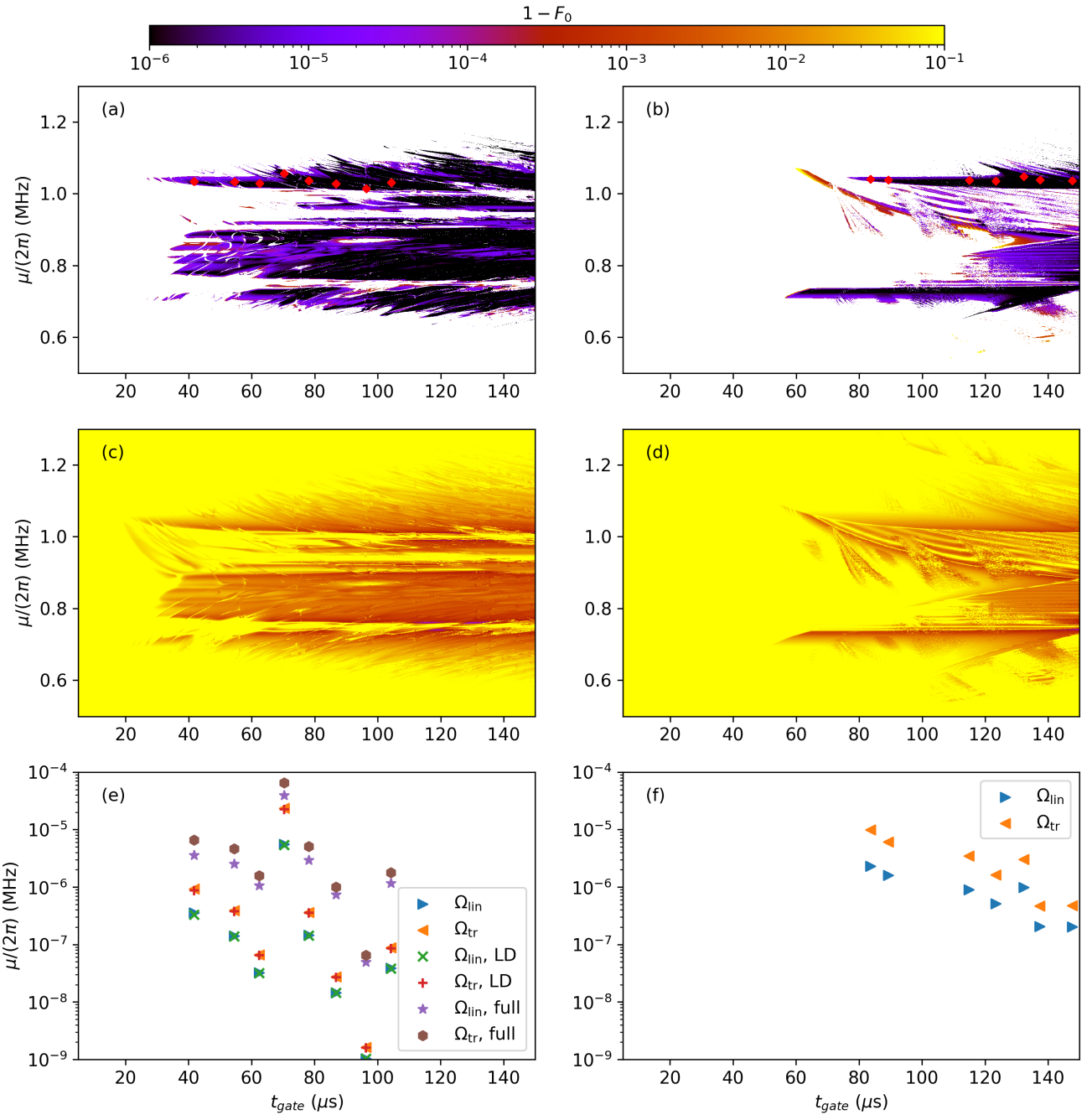


Figure 3. (a,b) Leading-order infidelity $1 - F_0$ (indicated by color) for transformed pulses Ω_{tr} inside the area (enclosed by solid line) where the inverse transformation \mathcal{S}^{-1} exists for 5-ion (a) and 20-ion (b) chains. The red points specify the values of (t_{gate}, μ) for which the simulations are performed. (c, d) Leading-order infidelity $1 - F_0$ for non-transformed pulses Ω_{lin} for 5-ion (a) and 20-ion (b) chains. (e) Spin flip error for the initial state $|11\rangle_x$ of a 5-ion chain with (t_{gate}, μ) specified by points in (a). For transformed and non-transformed pulses, it is calculated analytically and numerically with the Hamiltonian in Lamb-Dicke approximation and with the full Hamiltonian. (f) Analytical spin flip error for the initial state $|11\rangle_x$ of a 5-ion chain with (t_{gate}, μ) specified by points in (b).

exceed 10^{-4} , and it is even smaller for a 20-ion chain.

In addition, we perform numerical simulations for a selected set of points shown in Fig. 3(a) for a 5-ion chain. For each pair (t, μ) indicated by a point, we model gate

dynamics by solving TDSE with the pulses $\Omega_{\text{lin}}(t)$ and $\Omega_{\text{tr}}(t)$ for the initial states $|11\rangle_z$ and $|11\rangle_x$.

For the initial states $|11\rangle_x$, we calculate the spin flip error as in Section IV: we compared the simulations with

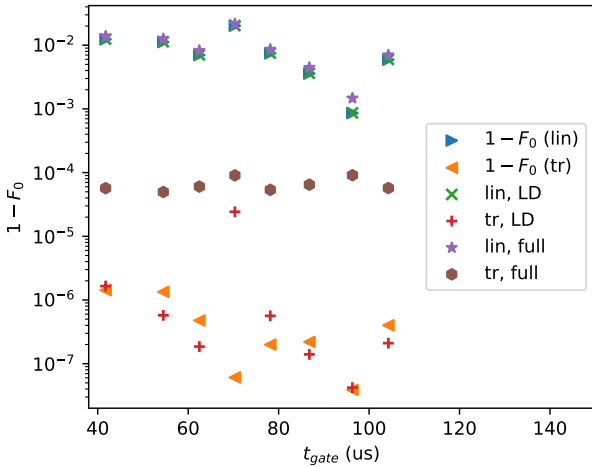


Figure 4. Leading-order infidelity $1 - F_0$ compared with the infidelity calculated from numerical simulation for the initial state $|11\rangle_z$ in 5-ion chain with t_{gate}, μ specified in Fig. 3(a). The values of $1 - F_0$ are compared with the simulation results for the Lamb-Dicke Hamiltonian and full Hamiltonian both for transformed and non-transformed pulses.

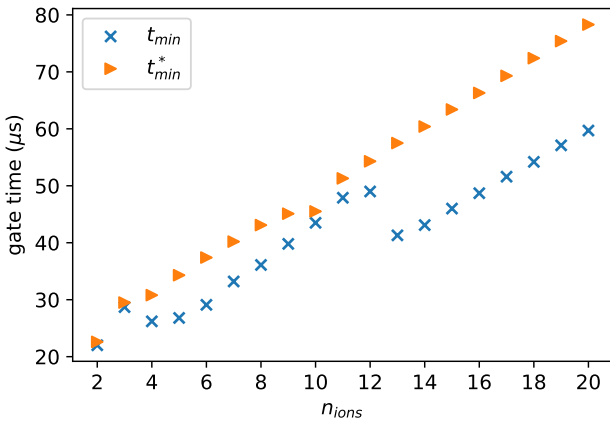


Figure 5. Minimal gate time t_{min} for which Ω_{eff} does not exceed $C\mu$ and minimal gate time t_{min}^* ensuring the zero-order error equal to 10^{-5} for optimized pulses and $|\psi_0\rangle = |11\rangle_z$ as functions of n_{ions} .

full Hamiltonian, with the Hamiltonian expanded up to the first order in Lamb-Dicke parameters, and the perturbation theory. The results of these simulations confirm the findings of the Section IV: perturbation theory gives an accurate result for the first-order Hamiltonian (2), but the spin flip probability P_{flip}^s is by order of mag-

nitude higher for the full Hamiltonian (1). Even for the full Hamiltonian, P_{flip}^s is of order 10^{-5} for most of the simulations.

For the initial states $|11\rangle_z$, we perform calculations similar to that Table I. We compare the analytical zero-order infidelity given by Eq. (24) with the infidelity obtained from TDSE. The results are presented in Fig. 4. For all points, the infidelity for the pulses Ω_{tr} is considerably lower than for Ω_{lin} . By comparing the numerical infidelities for the full Hamiltonian and the Hamiltonian in the first order of the Lamb-Dicke expansion, we conclude that the Eq. (24) gives a leading-order contribution to the error for Ω_{lin} , and the dominant contribution to the error for Ω_{tr} comes from the higher orders of the Lamb-Dicke expansion.

These results show that the conclusions of the section IV persist for a wide range of these parameters providing that t_{gate} and μ are within the allowed area. Also, the calculations prove that the zero-order error can be reliably used to estimate fidelity gain given by our scheme.

For gate times of tens of microseconds, our scheme allows to reduce the gate error from $\sim 10^{-2}$ for non-optimized pulses to $\sim 10^{-5}$. Thus, our scheme facilitates the implementation of fast high-fidelity MS gates in chains with tens of ions, which is crucial for speeding up trapped-ion quantum computation.

VI. CONCLUSIONS

We propose an amplitude-pulse-shaping method for the implementation of the Molmer-Sorensen entangling gate in linear chains of trapped-ion qubits. Our method allows to considerably reduce the error originating from carrier transition, which is always present in ions interaction with bichromatic external field. We show that a certain nonlinear transformation of the laser pulse allows to compensate the modification of the spin-dependent forces by carrier transition almost entirely, thus enabling a fast high-fidelity gate. For short ion chains, we show analytically and numerically that our method allows the fidelity gain is 2-3 orders of magnitude for gate times of 50-100 μs , with the resulting fidelity below $\sim 10^{-4}$. According to our analytical calculations, these conclusions persist for longer chains at least up to 20 ions.

ACKNOWLEDGMENTS

This work was supported by Rosatom in the framework of the Roadmap for Quantum computing (Contract No. 868-1.3- 15/15-2021).

- [2] J. I. Cirac and P. Zoller, Quantum computations with cold trapped ions, *Physical Review Letters* **74**, 4091 (1995).
- [3] A. Sørensen and K. Mølmer, Entanglement and quantum computation with ions in thermal motion, *Phys. Rev. A* **62**, 022311 (2000).
- [4] D. Leibfried, B. DeMarco, V. Meyer, D. Lucas, M. Barrett, J. Britton, W. M. Itano, B. Jelenković, C. Langer, T. Rosenband, and D. J. Wineland, Experimental demonstration of a robust, high-fidelity geometric two ion-qubit phase gate, *Nature* **422**, 412 (2003).
- [5] J. Mizrahi, B. Neyenhuis, K. Johnson, W. C. Campbell, C. Senko, D. Hayes, and C. Monroe, Quantum control of qubits and atomic motion using ultrafast laser pulses, *Applied Physics B* **10.1007/s00340-013-5717-6** (2013), arXiv:1307.0557 [physics.atom-ph].
- [6] G. Kirchmair, J. Benhelm, F. Zähringer, R. Gerritsma, C. F. Roos, and R. Blatt, Deterministic entanglement of ions in thermal states of motion, *New. J. Phys.* **11**, 023002 (2009) 10.1088/1367-2630/11/2/023002 (2008), arXiv:0810.0670 [quant-ph].
- [7] T. Choi, S. Debnath, T. Manning, C. Figgatt, Z.-X. Gong, L.-M. Duan, and C. Monroe, Optimal quantum control of multimode couplings between trapped ion qubits for scalable entanglement, *Physical Review Letters* **112**, 190502 (2014).
- [8] A. R. Milne, C. L. Edmunds, C. Hempel, F. Roy, S. Mavadia, and M. J. Biercuk, Phase-modulated entangling gates robust to static and time-varying errors, *Physical Review Applied* **13**, 024022 (2020).
- [9] Y. Shapira, R. Shaniv, T. Manovitz, N. Akerman, and R. Ozeri, Robust entanglement gates for trapped-ion qubits, *Physical Review Letters* **121**, 180502 (2018).
- [10] N. Grzesiak, R. Blümel, K. Wright, K. M. Beck, N. C. Pisenti, M. Li, V. Chaplin, J. M. Amini, S. Debnath, J.-S. Chen, and Y. Nam, Efficient arbitrary simultaneously entangling gates on a trapped-ion quantum computer, *Nature Communications* **11**, 10.1038/s41467-020-16790-9 (2020).
- [11] R. Blümel, N. Grzesiak, N. Pisenti, K. Wright, and Y. Nam, Power-optimal, stabilized entangling gate between trapped-ion qubits, *npj Quantum Information* **7**, 10.1038/s41534-021-00489-w (2021).
- [12] B. P. Ruzic, M. N. Chow, A. D. Burch, D. S. Lobser, M. C. Revelle, J. M. Wilson, C. G. Yale, and S. M. Clark, Leveraging motional-mode balancing and simply parametrized waveforms to perform frequency-robust entangling gates, *Physical Review Applied* **22**, 014007 (2024).
- [13] T. Olsacher, L. Postler, P. Schindler, T. Monz, P. Zoller, and L. M. Sieberer, Scalable and parallel tweezer gates for quantum computing with long ion strings, *PRX Quantum* **1**, 020316 (2020).
- [14] Y. Wu, S.-T. Wang, and L.-M. Duan, Noise analysis for high-fidelity quantum entangling gates in an anharmonic linear paul trap, *Phys. Rev. A* **97**, 062325 (2018).
- [15] S. S. Vedaie, E. J. Páez, N. H. Nguyen, N. M. Linke, and B. C. Sanders, Bespoke pulse design for robust rapid two-qubit gates with trapped ions, *Phys. Rev. Res.* **5**, 023098 (2023).
- [16] R. Blümel, A. Maksymov, and M. Li, Toward a mølmer sørensen gate with .9999 fidelity, *Journal of Physics B: Atomic, Molecular and Optical Physics* **57**, 205501 (2024).
- [17] C. F. Roos, Ion trap quantum gates with amplitude-modulated laser beams, *New Journal of Physics* **10**, 013002 (2008) 10.1088/1367-2630/10/1/013002 (2007), arXiv:0710.1204 [quant-ph].
- [18] D. James, Quantum dynamics of cold trapped ions with application to quantum computation, *Applied Physics B: Lasers and Optics* **66**, 181 (1998).
- [19] C. Monroe, W. Campbell, L.-M. Duan, Z.-X. Gong, A. Gorshkov, P. Hess, R. Islam, K. Kim, N. Linke, G. Pagano, P. Richerme, C. Senko, and N. Yao, Programmable quantum simulations of spin systems with trapped ions, *Reviews of Modern Physics* **93**, 025001 (2021).
- [20] P. C. Haljan, K.-A. Brickman, L. Deslauriers, P. J. Lee, and C. Monroe, Spin-dependent forces on trapped ions for phase-stable quantum gates and entangled states of spin and motion, *Physical Review Letters* **94**, 153602 (2005).
- [21] S.-L. Zhu, C. Monroe, and L.-M. Duan, Arbitrary-speed quantum gates within large ion crystals through minimum control of laser beams, *Europhysics Letters (EPL)* **73**, 485 (2006).
- [22] J. Johansson, P. Nation, and F. Nori, Qutip 2: A python framework for the dynamics of open quantum systems, *Computer Physics Communications* **184**, 1234 (2013).
- [23] M. A. Nielsen and I. L. Chuang, *Quantum Computation and Quantum Information* (Cambridge University Press, 2010).
- [24] M. O. Scully and M. S. Zubairy, *Quantum Optics* (Cambridge University Press, 1997).

Appendix A: Pulse shaping with piecewise-polynomial pulses

To implement the MS gate, one needs to find the pulse envelope $\Omega(t)$ which satisfies Eqs. (21). These equations comprise a system of $2n_{ions}$ linear and one quadratic equations on $\Omega(t)$.

Assume that $\Omega(t)$ is decomposed into a basis set $\{b_s(t)\}$, $\Omega(t) = \sum_s \Omega_s b_s(t)$, where the functions $b_s(t)$ are defined on the interval (t_0, t_f) of the gate duration. Then, the equations $\alpha_{im} = 0$ reduce to a linear system [14]

$$\sum_s A_{ms} \Omega_s = 0, \quad (A1)$$

where

$$A_{ms} = \int_{t_i}^{t_f} dt \Omega_s(t) \cos(\mu t + \psi) e^{i\omega_m t}, \quad (A2)$$

and the equation $\chi_{12}(t_f) = \phi$ reduces to a quadratic equation

$$\sum_{ss'} B_{ss'} \Omega_s \Omega_{s'} = \frac{\pi}{4}, \quad (A3)$$

where

$$B_{ss'} = - \sum_m 2\eta_{1m}\eta_{2m} \int_{t_i}^{t_f} dt \int_{t_i}^t dt' \Omega_s(t) \Omega_{s'}(t') \times \cos(\mu t + \psi) \cos(\mu t' + \psi) \sin[\omega_m(t - t')] \quad (A4)$$

In order to ensure the smoothness conditions necessary for the consideration of Section IV, we search for $\Omega(t)$ in form of a cubic spline defined by its values in the points t_s evenly spaced in the interval (t_0, t_f) , $t_s = t_0 + \frac{(t_f - t_0)s}{n_{seg} + 1}$, where $s = 0, \dots, n_{seg} + 1$. The basis functions $b_s(t)$ are defined as cubic splines on the interval (t_0, t_f) satisfying the boundary conditions $b_s(t_0) = b_s(t_f) = 0$, $b'_s(t_0) = b'_s(t_f) = 0$ and the conditions $b_s(t_{s'}) = \delta_{s,s'}$, $s = 1 \dots n_{seg}$.

Appendix B: MS gate fidelity with account for first-order spin-flip correction

In this Appendix, we derive expressions for the Molmer-Sorensen gate fidelity with account to three contributions: incompletely closed phonon mode phase trajectories, error in MS rotation angle, and spin-flip contribution. We consider fidelity in the full ion-phonon Hilbert space assuming that all phonon modes are initially cooled to the ground state. So, fidelity is defined as squared overlap between the target state and the resulting state:

$$F = |\langle \psi_0 | R_{XX}^\dagger(\phi) U | \psi_0 \rangle|^2. \quad (\text{B1})$$

To find F using perturbation theory, it is convenient to denote the combination $R_{XX}^\dagger(\phi) U$ as

$$R_{XX}^\dagger(\phi) U = 1 - i\hat{T}. \quad (\text{B2})$$

Using the unitarity of $R_{XX}^\dagger(\phi) U$, we can rewrite fidelity in the form more suitable for perturbative calculation:

$$1 - F = \langle \psi_0 | T^\dagger T | \psi_0 \rangle - \langle \psi_0 | T | \psi_0 \rangle^2. \quad (\text{B3})$$

Then, we use the MS gate propagator U with the first-order correction from the spin-flip perturbation (19). Let us give a small-error expansion of T . We assume that α_{im} and the deviation of χ_{ij} from the target values are small, so the MS propagator can be decomposed as

$$R_{XX}(\phi)^\dagger U_0 = \mathbb{1} - i\delta U_{\text{MS}}, \quad (\text{B4})$$

where

$$\delta U_{\text{MS}} \approx \frac{1}{2} \sum_{i,j} \chi_{ij} \sigma_x^i \sigma_x^j + i \sum_{im} \sigma_x^i (\alpha_{im}^* a_m - \alpha_{im} a_m^\dagger). \quad (\text{B5})$$

After that, \hat{T} can be approximated as

$$\hat{T} \approx \delta U_{\text{MS}} + \hat{T}_1, \quad (\text{B6})$$

where we define \hat{T}_1 by Eq.(20), and neglect the term $\delta U_{\text{MS}} T_1$. We find convenient to separate the contributions of δU_{MS} and \hat{T}_1 into gate infidelity. For that, we define two auxiliary fidelities. The first one is the fidelity of the state obtained by the action of the MS propagator (15),

$$F_0 = |\langle \psi_0 | R_{XX}^\dagger(\phi) U_0 | \psi_0 \rangle|^2 \quad (\text{B7})$$

It contains only the contributions of the imperfectly closed phase trajectories and the error in MS rotation angle. The second one is the fidelity between the states $U_0 | \psi_0 \rangle$ and $U | \psi_0 \rangle$:

$$F_c = |\langle \psi_0 | U_0^\dagger U | \psi_0 \rangle|^2 \quad (\text{B8})$$

It characterizes the deviation of the full evolution operator \hat{U} from the Molmer-Sorensen propagator (15) and is determined by \hat{T}_1 . Similarly with (B3), we can express F_0 and F_c as

$$1 - F_0 = \langle \psi_0 | \delta U_{\text{MS}}^\dagger \delta U_{\text{MS}} | \psi_0 \rangle - |\langle \psi_0 | \delta U_{\text{MS}} | \psi_0 \rangle|^2. \quad (\text{B9})$$

and

$$1 - F_c = \langle \psi_0 | T_1^\dagger T_1 | \psi_0 \rangle - |\langle \psi_0 | T_1 | \psi_0 \rangle|^2. \quad (\text{B10})$$

The auxiliary fidelities (B7), (B8) are helpful for analysing the fidelity (B1). First, the fidelity (B1) for any initial state can be bounded using the triangle inequality for fidelities [23]:

$$F > \cos(\arccos F_0 + \arccos F_c). \quad (\text{B11})$$

Then, let us prove that the infidelity (B3) averaged over initial states is simply a sum of (B9) and (B10). Indeed, the average of (B3) can be calculated as

$$1 - \langle F \rangle = \frac{1}{2^N} \left[\text{Tr}_q \langle 0_{ph} | T^\dagger T | 0_{ph} \rangle - \text{Tr}_q \langle 0_{ph} | T^\dagger | 0_{ph} \rangle \langle 0_{ph} | T | 0_{ph} \rangle \right], \quad (\text{B12})$$

where Tr_q denotes the trace over qubit space. Then, we substitute the Eq. (B6) into Eq. (B12). As δU_{MS} commutes with all σ_x^i , and \hat{T}_1 contains only terms flipping the pseudospin direction along the x axis, all cross-products of δU_{MS} and \hat{T}_1 vanish. Therefore, we get

$$1 - \langle F \rangle = (1 - \langle F_0 \rangle) + (1 - \langle F_c \rangle), \quad (\text{B13})$$

Using Eq. (B12), we get the following expression for $\langle F_0 \rangle$:

$$1 - \langle F_0 \rangle = \sum |\alpha_{im}|^2 + \frac{2^N}{2^N + 1} \sum_{i < j} \delta \chi_{ij}^2. \quad (\text{B14})$$

The contribution F_c averaged over initial states can be bounded from above as an average over all qubit basis states in the x -basis, which simply follows from Eq. (B12):

$$1 - F_c < \frac{1}{2^N} \text{Tr}_q T_1^\dagger T_1 = \frac{1}{2^N} \sum_s \langle s, 0_{ph} | T_1^\dagger T_1 | s, 0_{ph} \rangle. \quad (\text{B15})$$

A closed-form representation of the term $\langle s, 0_{ph} | T_1^\dagger T_1 | s, 0_{ph} \rangle$, which is the probability of a spin flip during the MS gate operation for the initial state $|s, 0_{ph} \rangle$, is given in Appendix C.

Now let us give expressions for some particular initial states. First of all, let us take the initial state of the

form $|s\rangle \otimes |0_{\text{ph}}\rangle$. Similarly with the average fidelity, the action of δU_{MS} and \hat{T}_1 in the qubit space implies that the infidelity is a sum of contributions from these operators. We get

$$1 - F_0 = \sum_m \left| \sum_i \alpha_{im} s_i \right|^2, \quad (\text{B16})$$

$$1 - F_c = \langle s, 0_{\text{ph}} | T_1^\dagger T_1 | s, 0_{\text{ph}} \rangle, \quad (\text{B17})$$

$$1 - F = \sum_m \left| \sum_i \alpha_{im} s_i \right|^2 + \langle s, 0_{\text{ph}} | T_1^\dagger T_1 | s, 0_{\text{ph}} \rangle. \quad (\text{B18})$$

Here $\delta\chi_{ij}$ does not contribute into error as it is responsible only for the phase between different qubit basis vectors in x -basis.

Finally, let us give expressions for F_0 for the initial state $|\psi_0\rangle = |s\rangle_z \otimes |0_{\text{ph}}\rangle$ (a spin string in z -basis) and for an arbitrary superposition of qubit states in x basis:

$$|\psi_0\rangle = \sum c_s |s\rangle \otimes |0_{\text{ph}}\rangle. \quad (\text{B19})$$

For $|\psi_0\rangle = |s\rangle_z \otimes |0_{\text{ph}}\rangle$,

$$1 - F_0 = \sum_{i < j} |\alpha_{im}|^2 + \sum_{i < j} \delta\chi_{ij}^2. \quad (\text{B20})$$

For a superposition with arbitrary coefficients c_s ,

$$1 - F_0 = \sum_s |c_s|^2 |\alpha^T s|^2 + \frac{1}{4} \sum_s |c_s|^2 (s^T \delta\chi s)^2 - \frac{1}{4} \left| \sum_s |c_s|^2 (s^T \delta\chi s) \right|^2. \quad (\text{B21})$$

The expressions for F_0 for the latter states can be obtained in the same way. In general, they contain the interference terms coming from products of δU_{MS} and \hat{T}_1 .

Appendix C: Spin flip probability

In this Appendix, we derive a closed-form representation of the probability of a spin flip during the MS gate operation for the initial state $|s, 0_{\text{ph}}\rangle$, which is given by the matrix element $\langle s, 0_{\text{ph}} | T_1^\dagger T_1 | s, 0_{\text{ph}} \rangle$. We represent it as a two-dimensional integral. From Eq. (20), we get

$$T_1^\dagger T_1 = \int dt' dt'' U_0^\dagger(t', t_0) \hat{V}(t') U_0(t', t'') \hat{V}(t'') U_0(t'', t_0). \quad (\text{C1})$$

The propagator U_0 given by Eq. (15) is diagonal in qubit space and contains displacement operators in phonon space and can be represented as

$$U_0(t_2, t_1) = \sum e^{-i\chi_s(t_2, t_1)} D(\alpha^T(t_2, t_1)s) |s\rangle \langle s|, \quad (\text{C2})$$

where $\alpha(t_2, t_1)$ is the matrix $\alpha_{im}(t_2, t_1)$, and

$$\chi_s(t_2, t_1) = \frac{1}{2} \sum_{ij} \chi_{ij}(t_2, t_1) s_i s_j. \quad (\text{C3})$$

The perturbation \hat{V} can be written as

$$\hat{V}(t) = \sum \hat{V}_m^\beta(t) A_m^\beta, \quad \beta = 1, 2, \quad (\text{C4})$$

with

$$A_m^1 = \hat{a}_m, \quad A_m^2 = \hat{a}_m^\dagger, \quad (\text{C5})$$

$$V_m^\beta(t) = \sum_i V_{im}^\beta(t) \sigma_z^i, \quad (\text{C6})$$

$$V_{im}^{1,2}(t) = \eta_{im} \Omega(t) \cos(\mu t + \psi) \sin 2\Phi(t) e^{\mp i\omega_m t}. \quad (\text{C7})$$

By substituting these expressions into Eq. (C1) and taking the required matrix element, one gets

$$\langle s, 0_{\text{ph}} | T_1^\dagger T_1 | s, 0_{\text{ph}} \rangle = \sum_{i, m_1, m_2, \beta_1, \beta_2, s'} \int dt_1 dt_2 (V_{m_1}^{\beta_1})_{ss'}(t_1) (V_{m_2}^{\beta_2})_{ss'}(t_2) e^{i(\chi_s(t_1, t_0) - \chi_{s'}(t_1, t_2) + \chi_s(t_2, t_0))} \langle 0_{\text{ph}} | D^\dagger(\alpha^T(t_1, t_0)s) \hat{A}_{m_1}^{\beta_1} D(\alpha^T(t_1, t_2)s') \hat{A}_{m_2}^{\beta_2} D(\alpha^T(t_2, t_0)s) | 0_{\text{ph}} \rangle. \quad (\text{C8})$$

The matrix elements of the products of displacement operators and creation and annihilation operators can be calculated using the identities for displacement operators which can be found in quantum optics textbooks (see,

for example, [24]). Below we give the expressions for the matrix elements for all combinations of β , which corresponds to all combinations of creation and annihilation operators:

$$\begin{aligned}
\langle 0_{\text{ph}} | D^\dagger(\vec{\alpha}) \hat{a}_{m_1} D(\vec{\alpha}_2) \hat{a}_{m_2} D(\vec{\alpha}_3) | 0_{\text{ph}} \rangle &= \langle 0_{\text{ph}} | D^\dagger(\vec{\alpha}_1) D(\vec{\alpha}_2) D(\vec{\alpha}_3) | 0_{\text{ph}} \rangle ((\alpha_2)_{m_1} + (\alpha_3)_{m_1})(\alpha_3)_{m_2}, \\
\langle 0_{\text{ph}} | D^\dagger(\vec{\alpha}_1) \hat{a}_{m_1} D(\vec{\alpha}_2) \hat{a}_{m_2}^\dagger D(\vec{\alpha}_3) | 0_{\text{ph}} \rangle &= \langle 0_{\text{ph}} | D^\dagger(\vec{\alpha}_1) D(\vec{\alpha}_2) D(\vec{\alpha}_3) | 0_{\text{ph}} \rangle (\alpha_1^*)_{m_1} (\alpha_3)_{m_3}, \\
\langle 0_{\text{ph}} | D^\dagger(\vec{\alpha}_1) \hat{a}_{m_1}^\dagger D(\vec{\alpha}_2) \hat{a}_{m_2} D(\vec{\alpha}_3) | 0_{\text{ph}} \rangle &= \langle 0_{\text{ph}} | D^\dagger(\vec{\alpha}_1) D(\vec{\alpha}_2) D(\vec{\alpha}_3) | 0_{\text{ph}} \rangle (\delta_{m_1 m_2} + ((\alpha_1)_{m_2}^* - (\alpha_2)_{m_2}^*) ((\alpha_2)_{m_1} + (\alpha_3)_{m_1})), \\
\langle 0_{\text{ph}} | D^\dagger(\vec{\alpha}_1) \hat{a}_{m_1}^\dagger D(\vec{\alpha}_2) \hat{a}_{m_2}^\dagger D(\vec{\alpha}_3) | 0_{\text{ph}} \rangle &= \langle 0_{\text{ph}} | D^\dagger(\vec{\alpha}_1) D(\vec{\alpha}_2) D(\vec{\alpha}_3) | 0_{\text{ph}} \rangle (\alpha_1)_{m_1}^* ((\alpha_1)_{m_2}^* - (\alpha_2)_{m_2}^*), \\
\langle 0_{\text{ph}} | D^\dagger(\vec{\alpha}_1) D(\vec{\alpha}_2) D(\vec{\alpha}_3) | 0_{\text{ph}} \rangle &= \exp \left\{ -i \text{Im}[(\vec{\alpha}_1 \vec{\alpha}_2^*) + (\vec{\alpha}_1 \vec{\alpha}_3^*) - (\vec{\alpha}_2 \vec{\alpha}_3^*)] - \frac{1}{2} |\alpha_1 - \alpha_2 - \alpha_3|^2 \right\}.
\end{aligned} \tag{C9}$$

Appendix D: Derivation of the expression for effective $\Omega(t)$

The integrals for α_{im} and χ_{ij} entering the MS propagator (Eqs. (16) and (17)) contain the term f_{im} (Eq.(18)) which contains a fastly-oscillating $\cos 2\Phi(t)$ term as a multiplier. Here we show how the fast oscillations can be approximately averaged to get rid of the nonlinear dependence on $\Omega(t)$. For that, let us rewrite f_{im} in the following way:

$$f_{im}(t) = \underbrace{\frac{1}{2} \eta_{im} e^{i(\omega_m - \mu)t - i\psi} \Omega(t)}_{\text{slow part}} \underbrace{(1 + e^{2i(\mu t + \psi)}) \cos 2\Phi(t)}_{\text{fast part}} \tag{D1}$$

With underbraces, we show the parts which we consider as slowly (fastly) varying. We assume that the slow part does not change significantly over several periods of carrier oscillations μ^{-1} . Then, we can average the fast part assuming that $\Omega(t)$ is approximately constant. Also, due to the assumptions on $\Omega(t)$ made in Section IV, we can replace $\Phi(t)$ by the leading-order asymptotic contribu-

tion:

$$\Phi(t) = \int_{t_i}^t dt' \Omega(t') \cos(\mu t' + \psi) \approx \frac{\Omega(t) \sin \mu t + \psi}{\mu}. \tag{D2}$$

After that, the fast part can be averaged as follows:

$$\begin{aligned}
\left\langle (1 + e^{2i(\mu t + \psi)}) \cos \left(\frac{2\Omega}{\mu} \sin(\mu t + \psi) \right) \right\rangle &= \\
&= J_0 \left(\frac{2\Omega}{\mu} \right) + J_2 \left(\frac{2\Omega}{\mu} \right), \tag{D3}
\end{aligned}$$

where J_n are Bessel functions. For constant $\Omega(t)$, this have been done in [17].

By substituting (D3) into (D1), we get

$$\begin{aligned}
f_{im}(t) &\approx \frac{1}{2} \eta_{im} e^{i(\omega_m - \mu)t - i\psi} \Omega(t) \times \\
&\quad \underbrace{\left(J_0 \left(\frac{2\Omega(t)}{\mu} \right) + J_2 \left(\frac{2\Omega(t)}{\mu} \right) \right)}_{\text{averaged fast part}} \tag{D4}
\end{aligned}$$

Due to smooth time dependence of $\Omega(t)$, we can replace the oscillating exponent with the cosine and obtain the Eq. (29).